

# Supporting Information

## **Discovery of two types of new porphyrin-C<sub>70</sub> co-crystals: influence of intermolecular contact on the inherent resistance**

Weidong Yu,<sup>a</sup> Qianwen Yan,<sup>a</sup> Yanmei Nie,<sup>a</sup> Shuang Liang,<sup>a</sup> Sanghao Li,<sup>a</sup> Yin Zhang,<sup>a</sup> Mingyuan Lin,<sup>a</sup> and Jun Yan\*

<sup>a</sup> School of Chemistry and Chemical Engineering, Central South University, Changsha 410083, China. E-mail: yanjun@csu.edu.cn.

<sup>b</sup> Hunan Provincial Key Laboratory of Efficient and Clean Utilization of Manganese Resource, Central South University, Changsha 410083, China.

# Table of contents

- 1. TGA and DSC analysis**
- 2. Single-crystal XRD data**
- 3.  $^1\text{H}$  NMR spectra.**
- 4. ESI-MS spectra.**
- 5. Data about IR**
- 6. UV-vis titration and Fluorescence spectra**
- 7. Powder X-ray diffraction analysis.**
- 8. Electrochemistry data**
- 9. The examples of different packing models**

## 1. TGA and DSC analysis

Because some solvent molecules have disordered structure in single crystal, the number of solvent molecules cannot be determined completely from single crystal XRD test. Therefore, TGA-DSC data and single crystal data are often used together to analyze the molecular formula. For the amounts of solvent molecule CS<sub>2</sub> of compounds **1**, **2** and **3**, we mainly determined from the weight loss ratio of the first stage in TGA and the endpoint of the weight lost was determined by DSC data. In addition, large molecular solvents such as *n*-hexane do not present this problem compared to small molecular solvents.

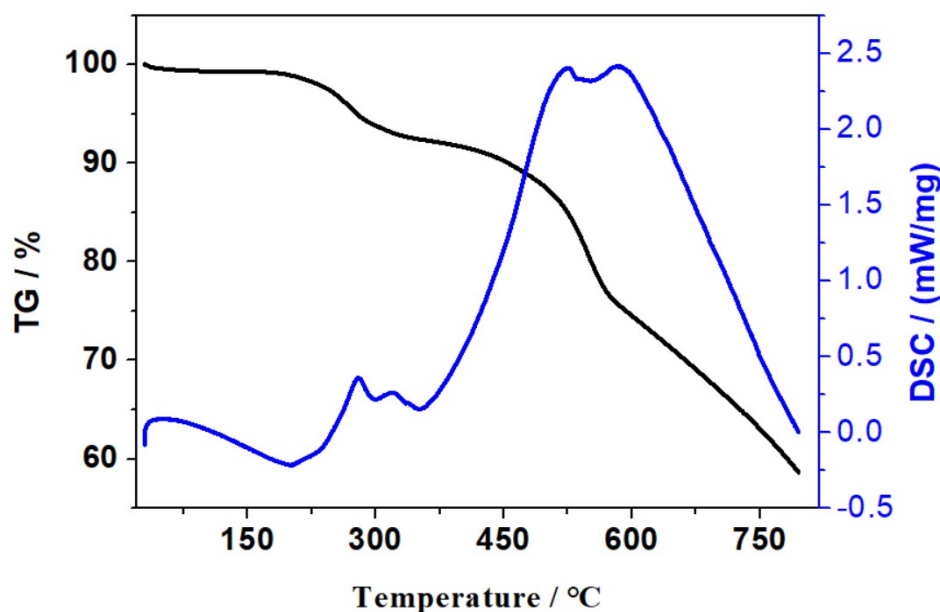


**Figure S1.** TGA and DSC analysis of compound **1**.

The TG curve shows three consecutive weight loss stages in the entire temperature range. The simultaneous TG-DSC data for compound **1** evolved that, in the first stage, a mass of weight (8.12 %) was desorbed corresponding to the loss of the solvent CS<sub>2</sub> at round 180°C. Hence, the formula of compound **1** was obtained as C<sub>44</sub>H<sub>28</sub>N<sub>4</sub>Co·C<sub>70</sub>·1.5CS<sub>2</sub>.

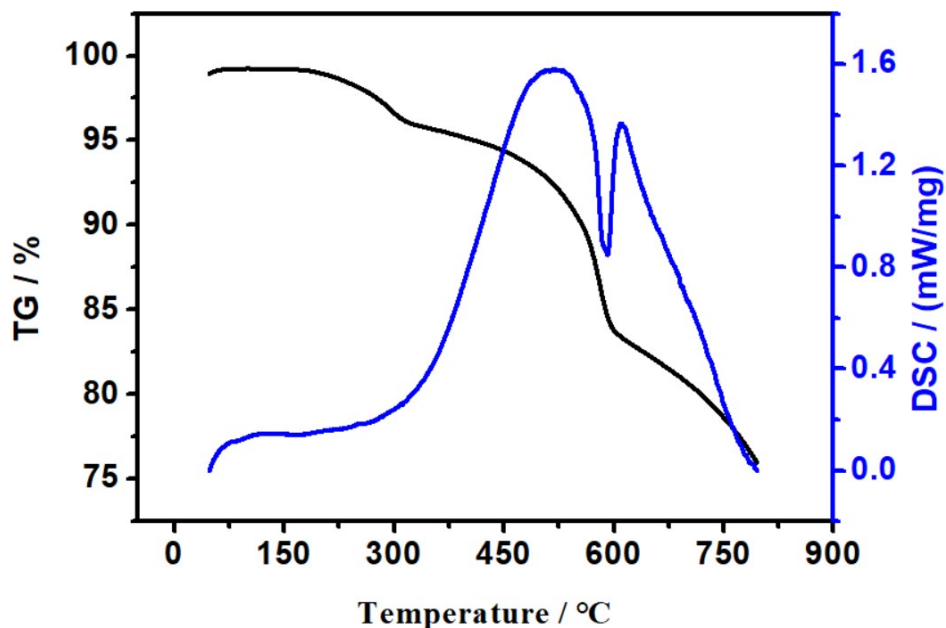


**Figure S2.** TGA and DSC analysis of compound **2**.

The TG curve shows three consecutive weight loss stages in the entire temperature range. The simultaneous TG-DSC data for compound **2** evolved that, in the first stage, a mass of weight (4.29 %) was desorbed corresponding to the loss of the solvent CS<sub>2</sub> at round 180°C. Hence, the formula of compound **1** was obtained as C<sub>44</sub>H<sub>28</sub>N<sub>4</sub>Zn·C<sub>70</sub>·CS<sub>2</sub>.

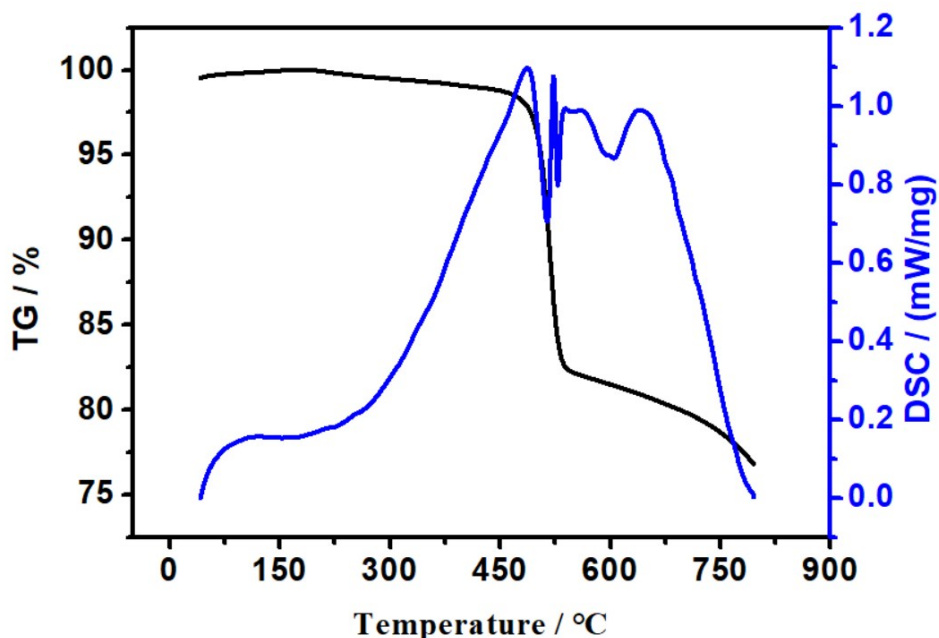


**Figure S3.** TGA and DSC analysis of compound **3**.

The TG curve shows two consecutive weight loss stages in the entire temperature range. The simultaneous TG-DSC data for compound **3** evolved that, in the first stage, a mass of weight (3.12 %) was desorbed corresponding to the loss of the solvent CS<sub>2</sub>

at round 180°C. Hence, the formula of compound **1** was obtained as  $C_{44}H_{28}N_4H_2 \cdot C_{70} \cdot CS_2$ .

## 2. Single-crystal XRD data

**Table S1.** Crystallographic data for compounds **1-3**.

Compound	<b>1</b>	<b>2</b>	<b>3</b>
Formula	$C_{231}H_{56}Co_2N_8S_6$	$C_{230}H_{56}N_8S_4Zn_2$	$C_{230}H_{60}N_8S_4$
Formula weight	3253.05	3189.80	3063.10
CCDC	1875457	1872220	1875456
Crystal system	Orthorhombic	Triclinic	Triclinic
Space group	Pnma	P -1	P -1
a, Å	25.4112(5)	17.4662(4)	17.4771(7)
b, Å	23.8293(4)	19.7085(4)	19.6561(7)
c, Å	22.1557(4)	20.6330(5)	20.6533(7)
$\alpha$ , °	90	85.483(2)	85.686(2)
$\beta$ , °	90	68.312(2)	68.147(2)
$\gamma$ , °	90	89.088(2)	89.352(2)
V, Å <sup>3</sup>	13416.0(4)	6578.6(3)	6565.5(4)
Z	4	2	2
T, K	293(2)	150(2)	296(2)
$D_{\text{calcd}}$ , g cm <sup>-3</sup>	1.611	1.610	1.549
$\mu$ , mm <sup>-1</sup>	0.419	1.659	0.151
Data / restraints / parameters	13514 / 0 / 1135	24725 / 200 / 2115	24026 / 2003 / 2155
Goodness-of-fit on F <sup>2</sup>	1.025	1.037	1.087
Final R indices [I > 2sigma(I)]	R <sub>1</sub> = 0.0405, wR <sub>2</sub> = 0.0984	R <sub>1</sub> = 0.0980, wR <sub>2</sub> = 0.2475	R <sub>1</sub> = 0.1021, wR <sub>2</sub> = 0.2605
R indices (all data)	R <sub>1</sub> = 0.0559, wR <sub>2</sub> = 0.1066	R <sub>1</sub> = 0.1081, wR <sub>2</sub> = 0.2578	R <sub>1</sub> = 0.1624, wR <sub>2</sub> = 0.2921

### 3. $^1\text{H}$ NMR spectra.

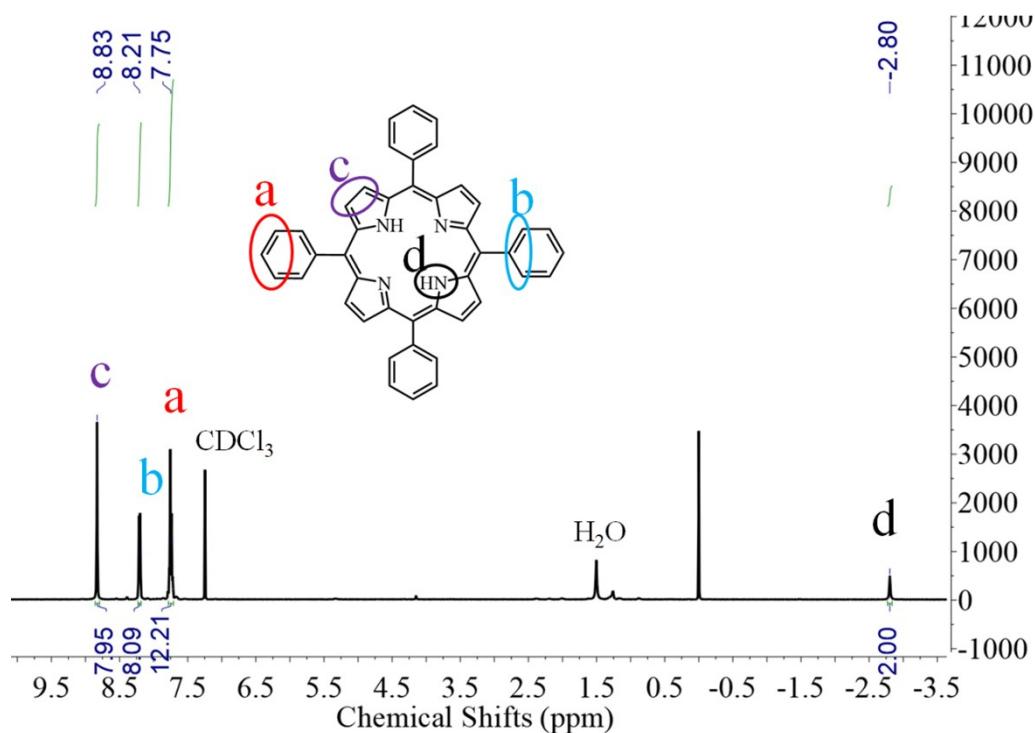


**Figure S4.**  $^1\text{H}$  NMR spectrum of  $\text{H}_2\text{TPP}$  ( $\text{CDCl}_3/\text{CS}_2 = 1/1$ , 400 MHz): 8.83 (s, 8 H), 8.21 (d, 8 H), 7.75 (m, 12 H), 2.80 (s, 2H) ppm.

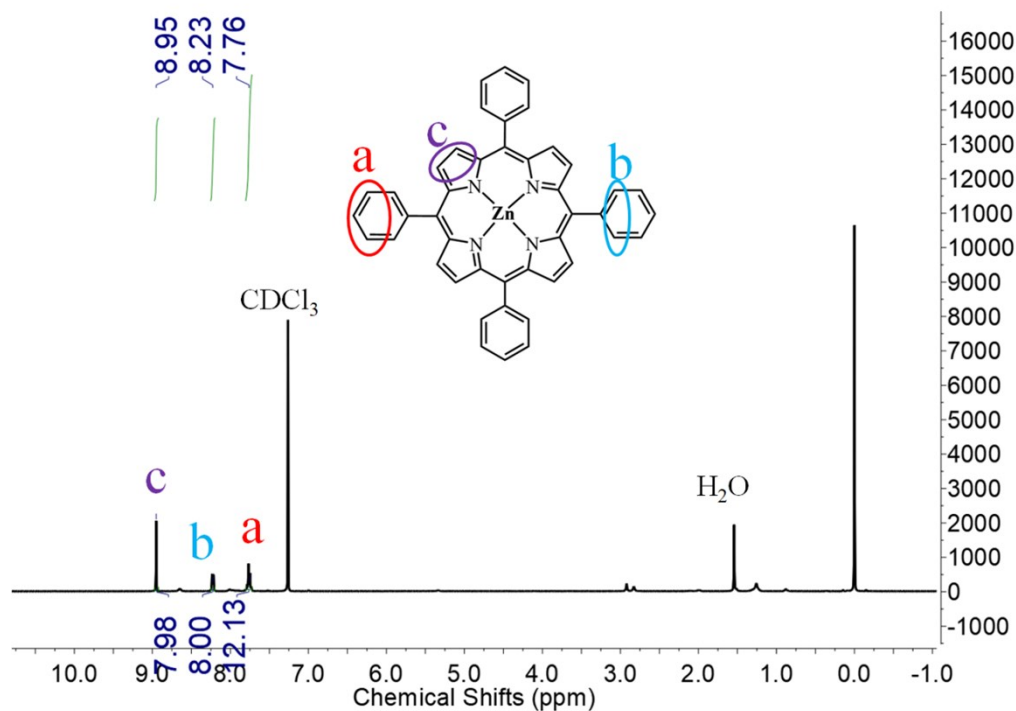


**Figure S5.**  $^1\text{H}$  NMR spectrum of  $\text{ZnTPP}$  ( $\text{CDCl}_3/\text{CS}_2 = 1/1$ , 400 MHz): 8.95 (s, 8 H), 8.23 (d, 8 H), 7.76 (m, 12 H) ppm.

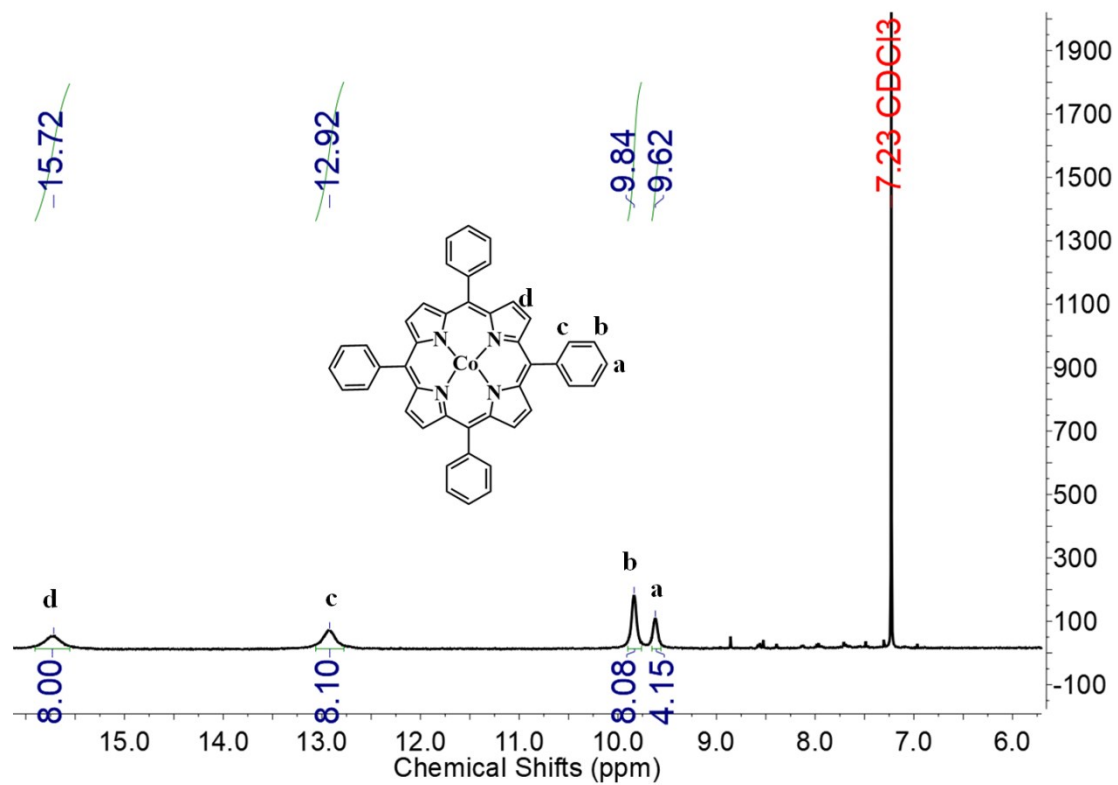


**Figure S6.**  $^1\text{H}$  NMR spectrum of CoTPP ( $\text{CDCl}_3/\text{CS}_2 = 1/1$ , 400 MHz): 15.72 (s, 8 H), 12.92 (d, 8 H), 9.84 (s, 8 H), 9.62 (s, 4 H) ppm.

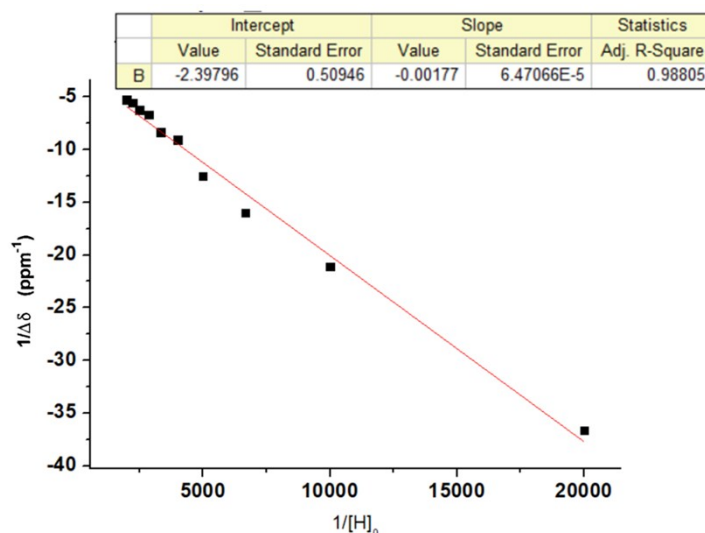


**Figure S7.** Benesi-Hildebrand data treatment of Co(TPP)-C<sub>70</sub>.

As shown in Figure 4, B-H equation (equation S1) was used to calculate the binding constant.

$$1/\Delta\delta = 1/(K \cdot \Delta\delta_{\max} \cdot [H]_0) + 1/\Delta\delta_{\max} \quad (\text{S1})$$

Where  $\Delta\delta = (\delta_G - \delta_{\text{obs}})$ ;

$$\Delta\delta_{\max} = (\delta_G - \delta_{\text{HG}});$$

$\delta_{\text{obs}}$  is an experimentally measured chemical shift;

$\delta_G$  is the chemical shift of a nucleus in the guest molecule;

$\delta_{\text{HG}}$  is the chemical shift of a nucleus in the host-guest compound;

$\Delta\delta$  is the measured change in chemical shift (upon addition of host species) referenced to that of the uncomplexed guest;

$\Delta\delta_{\max}$  is the difference in chemical shifts between that observed in the guest molecule and that observed in the host-guest compound;

$[H]$  is the concentration of host at equilibrium;

$K$  is the binding constant.

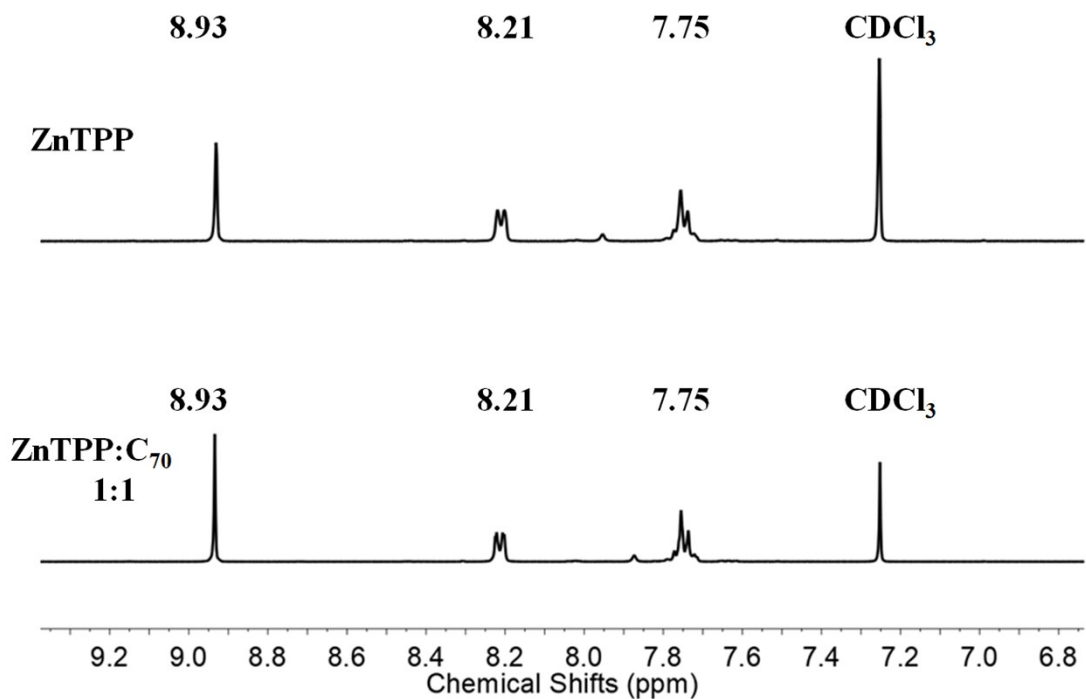


**Figure S8.**  $^1\text{H}$  NMR titration of ZnTPP- $\text{C}_{70}$  performed in  $\text{CDCl}_3/\text{CS}_2$  (volume ratio = 1/1) at room temperature. Addition  $\text{C}_{70}$  (each 0.1 mM) into ZnTPP solution (1 mM).

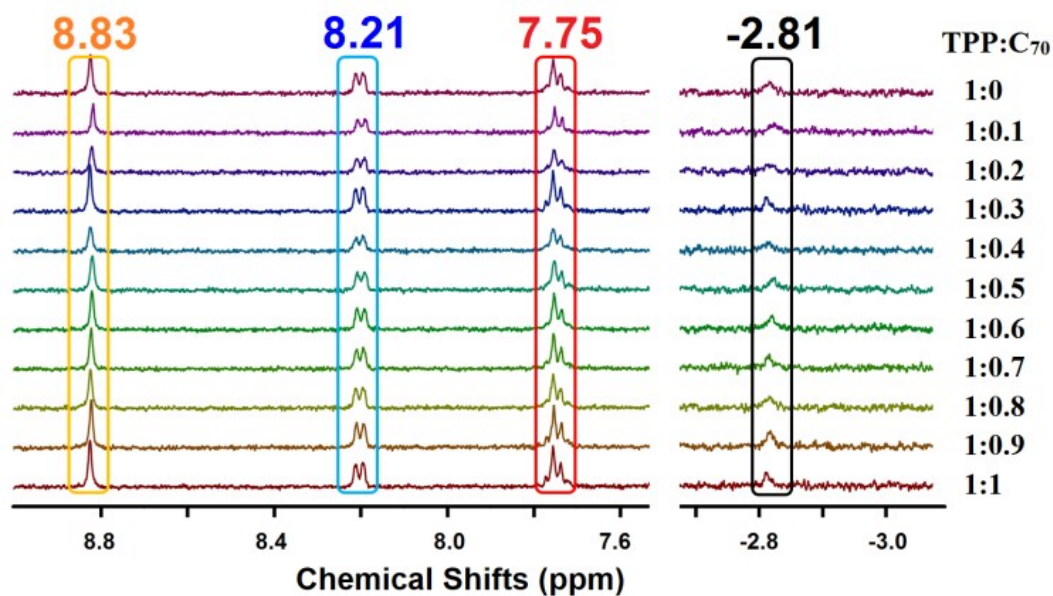


**Figure S9.**  $^1\text{H}$  NMR titration of  $\text{H}_2\text{TPP}-\text{C}_{70}$  performed in  $\text{CDCl}_3/\text{CS}_2$  (1/1) at room temperature. Addition  $\text{C}_{70}$  (each 0.05 mM) into  $\text{H}_2\text{TPP}$  solution (0.5 mM).

#### 4. ESI-MS spectra.

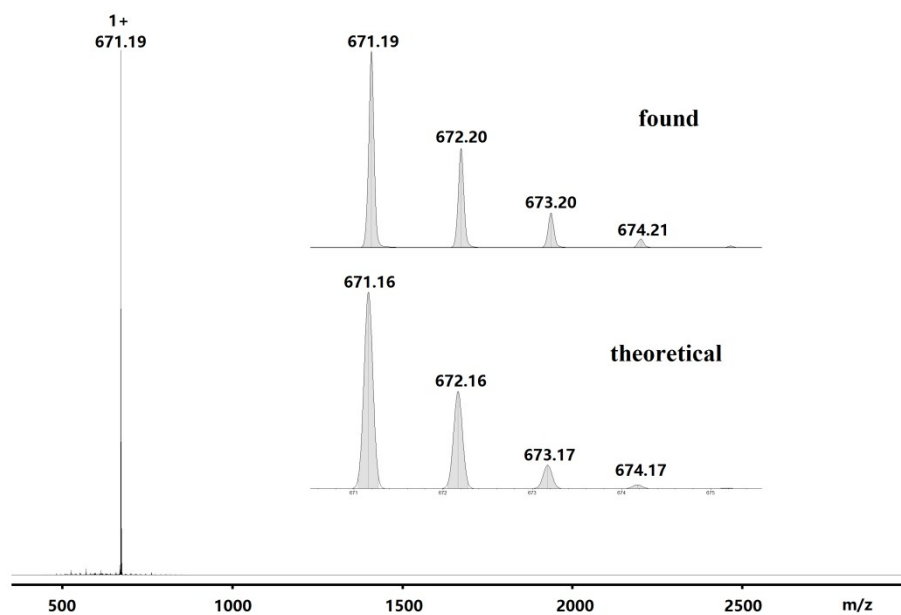


**Figure S10.** ESI-MS spectrum of CoTPP in  $\text{CH}_2\text{Cl}_2/\text{CH}_3\text{CN}$ . (Insert) Found:  $[\text{CoC}_{44}\text{H}_{30}\text{N}_4]^+$ , 671.19; theoretical: 671.16.

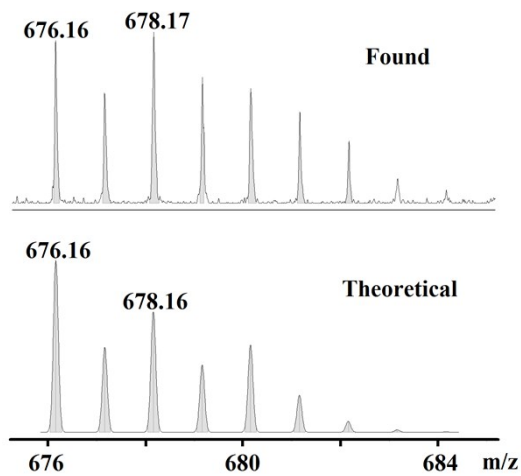


**Figure S11.** ESI-MS spectrum of ZnTPP in  $\text{CH}_2\text{Cl}_2/\text{CH}_3\text{CN}$ . Found:  $[\text{ZnC}_{44}\text{H}_{30}\text{N}_4]^+$ , 676.16; theoretical: 676.16.



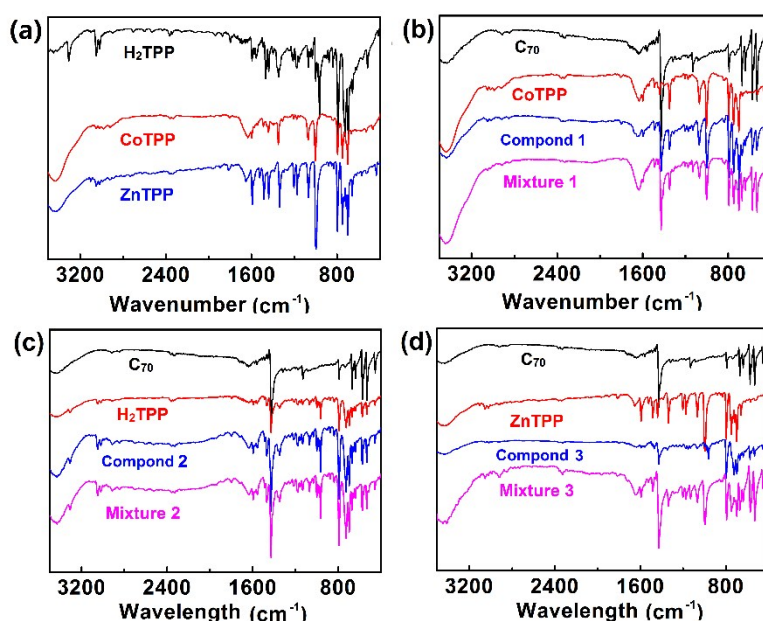


**Figure S13.** (a) IR spectra of MTPP (M = H<sub>2</sub>, Co and Zn); (b) IR spectra of C<sub>70</sub>, CoTPP, compound **1** and Mixture **1**; (c) IR spectra of C<sub>70</sub>, H<sub>2</sub>TPP, compound **3** and Mixture **3**; (d) IR spectra of C<sub>70</sub>, ZnTPP, compound **2** and Mixture **2**.

The IR spectra are used to compare the vibrational bands from MTPP (M = Co, Zn and H<sub>2</sub>), C<sub>70</sub> and their co-crystallized products. As shown in Figure S13, the peak at 3439 cm<sup>-1</sup> which can be assigned to the vibration of N-H band of pyrrole rings is vanished when coordinated with Zn or Co. The vibration bands at fingerprint region are also showed some shifts (see Table S2). Compared with the peaks of C<sub>70</sub> and MTPP (M = H<sub>2</sub>, Zn and Co), the peaks of corresponding compound (**1**, **2** and **3**) which can be assigned to C-C bond (about 700-800 cm<sup>-1</sup>) and C-H bond (about 3000-3100 cm<sup>-1</sup>) show obviously shifts. For comparison, MTPP and C<sub>70</sub> mixture were grinded as corresponding mixture. The specific details about the vibration peaks of different compounds were shown in Table S2. Different with co-crystallization compounds, the mixture does not show any shifts compared with C<sub>70</sub> and MTPP. These results suggest that the interaction between MTPP and C<sub>70</sub> is formed after co-crystallization from solution. Exactly as their crystal structures, the distorted porphyrins are also shown the interaction in solid phase.

## 6. UV-vis titration and Fluorescence spectra

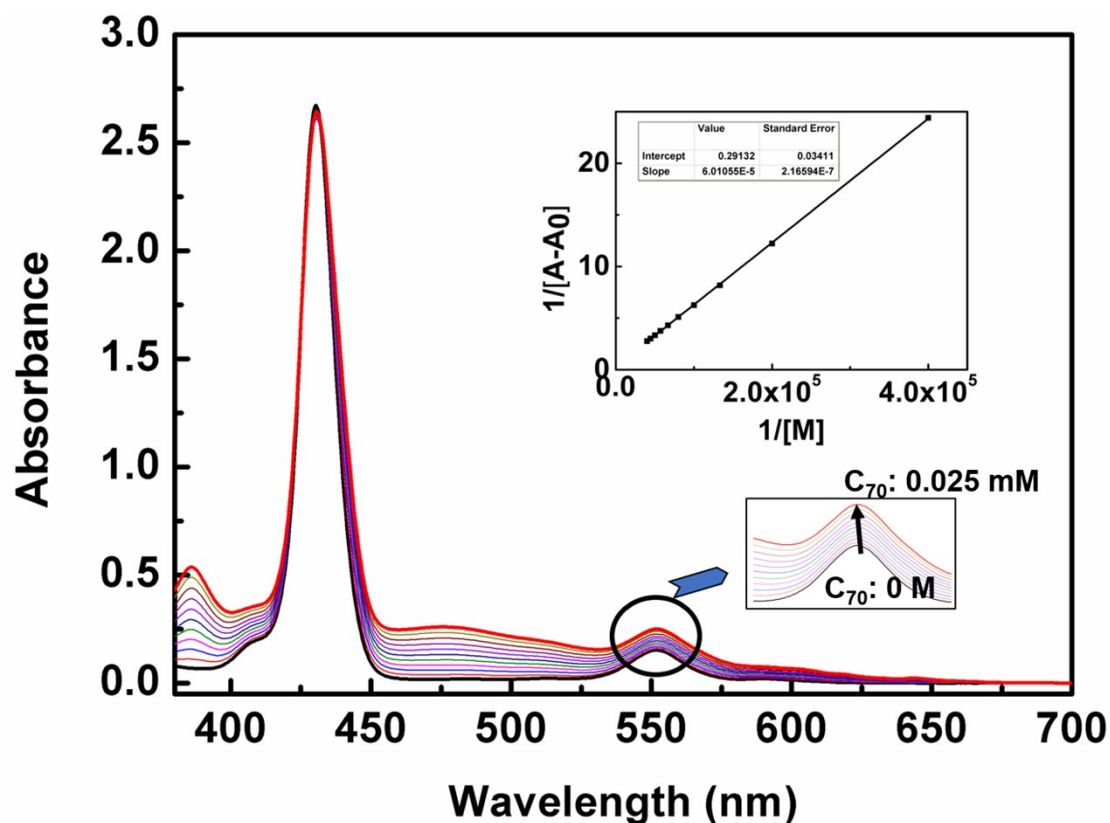


Figure S14. UV-vis absorption titration of ZnTPP ( $2.5 \times 10^{-5}$  M) on increasing addition  $C_{70}$  (each  $2.5 \times 10^{-6}$  M) in  $CS_2$ . (Insertion) B-H equation at about 551 nm.

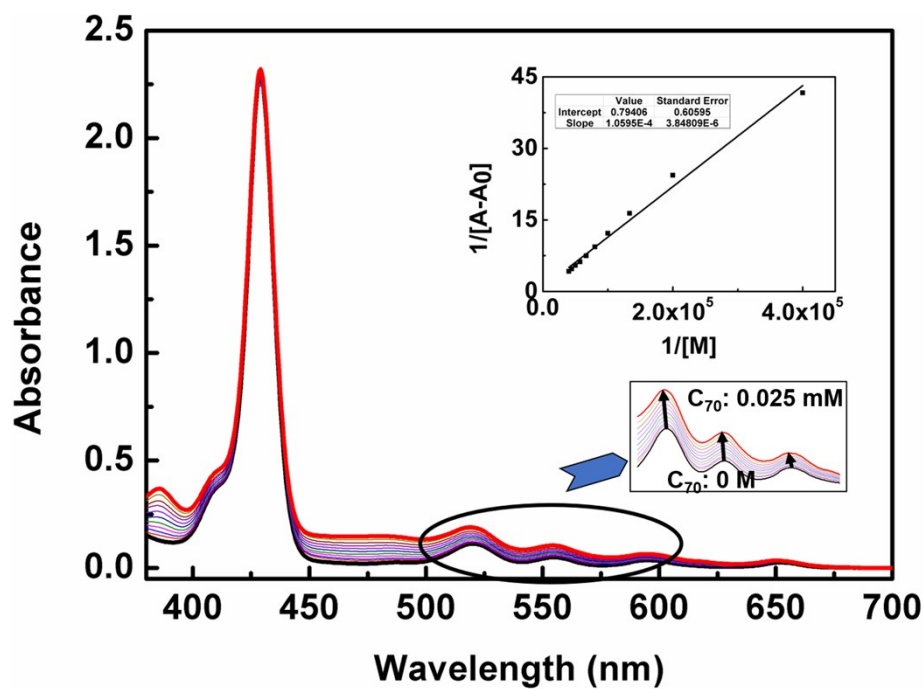
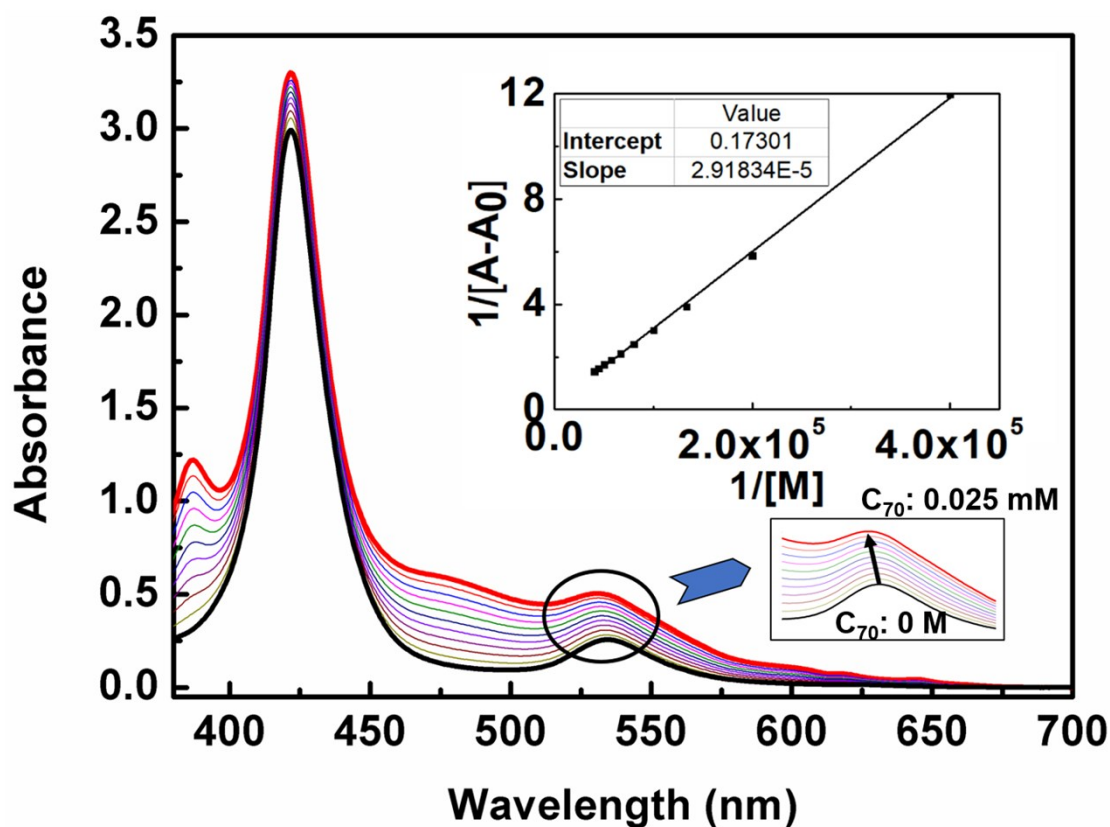


Figure S15. UV-vis absorption titration of  $H_2TPP$  ( $2.5 \times 10^{-5}$  M) on increasing addition  $C_{70}$  (each  $2.5 \times 10^{-6}$  M) in  $CS_2$ . (Insertion) B-H equation at about 514 nm.



**Figure S16.** UV-vis absorption titration of CoTPP ( $2.5 \times 10^{-5}$  M) on increasing addition  $C_{70}$  (each  $2.5 \times 10^{-6}$  M) in  $CS_2$ . (Insertion) B-H equation at about 526 nm.

The binding constant  $K$  were determined from the following B-H equation (S2):

$$\frac{1}{A - A_0} = \frac{a}{a - b} \cdot \left[ \frac{1}{K[M]} + 1 \right] \quad (S2)$$

Where  $K$  = binding constant;

$A_0$  = the observed absorption in the absence of cation;

$A$  = the observed absorption the cation-added;

$[M]$  = the concentration of the cation-added;

$a$  and  $b$  are constants, the binding constant value  $K$  was evaluated graphically by plotting  $1/(A-A_0)$  against  $1/[M]$ .

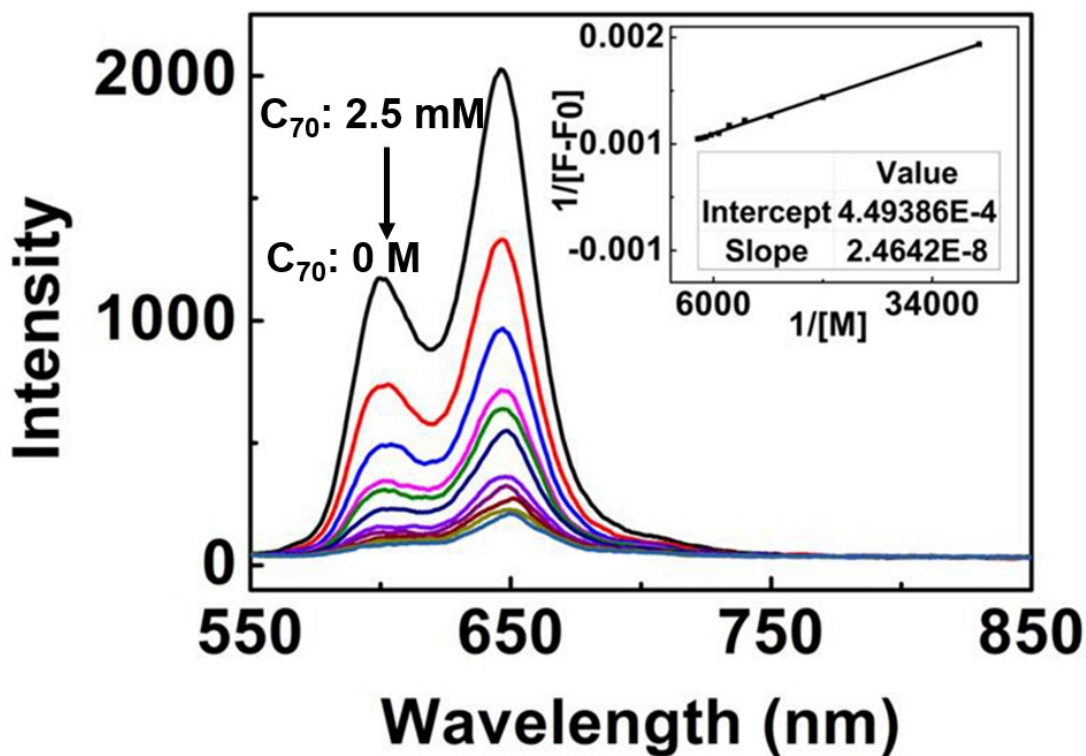


**Figure S17.** Fluorescence spectrum titration of  $\text{H}_2\text{TPP}$  ( $2.5 \times 10^{-3} \text{ M}$ ) upon increasing addition  $\text{C}_{70}$  (each  $2.5 \times 10^{-4} \text{ M}$ ) in  $\text{CS}_2$  solution. (Insertion) B-H equation. The fluorescence experiment was carried at 430 nm excitation wavelength.

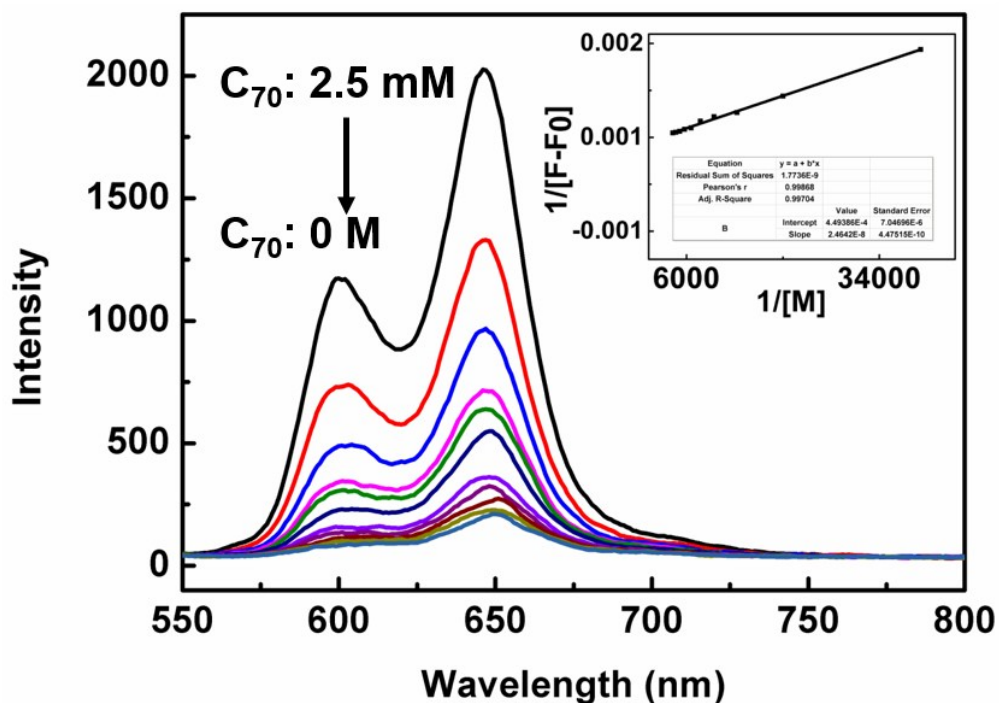


**Figure S18.** Fluorescence spectra titration of  $\text{ZnTPP}$  ( $2.5 \times 10^{-3} \text{ M}$ ) upon increasing addition  $\text{C}_{70}$  (each  $2.5 \times 10^{-4} \text{ M}$ ) in  $\text{CS}_2$  solution. (Insertion) B-H equation. The fluorescence experiment was carried at 430 nm excitation wavelength.

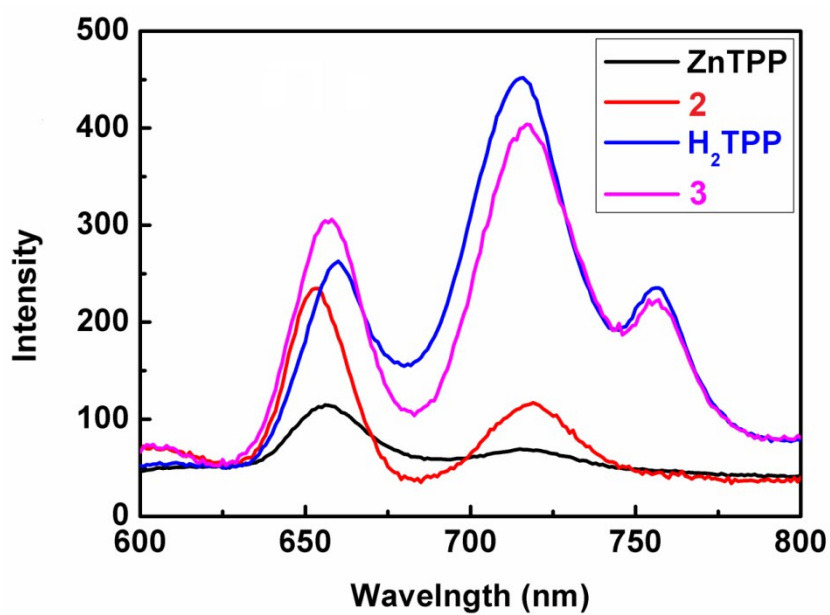


**Figure S19.** Solid-stated fluorescence spectra of ZnTPP, compound 3, H<sub>2</sub>TPP and compound 2. The fluorescence experiment was carried at 430 nm excitation wavelength.

The binding constant  $K$  were determined from the following B-H equation (S3):

$$\frac{1}{F - F_0} = \frac{a}{a - b} \cdot \left[ \frac{1}{K[M]} + 1 \right] \quad (\text{S3})$$

Where  $K$  = binding constant;

$F_0$  = the observed fluorescence in the absence of cation;

$F$  = the observed fluorescence the cation-added;

$[M]$  = the concentration of the cation-added;

$a$  and  $b$  are constants, the binding constant value  $K$  was evaluated graphically by plotting  $1/(F-F_0)$  against  $1/[M]$ .

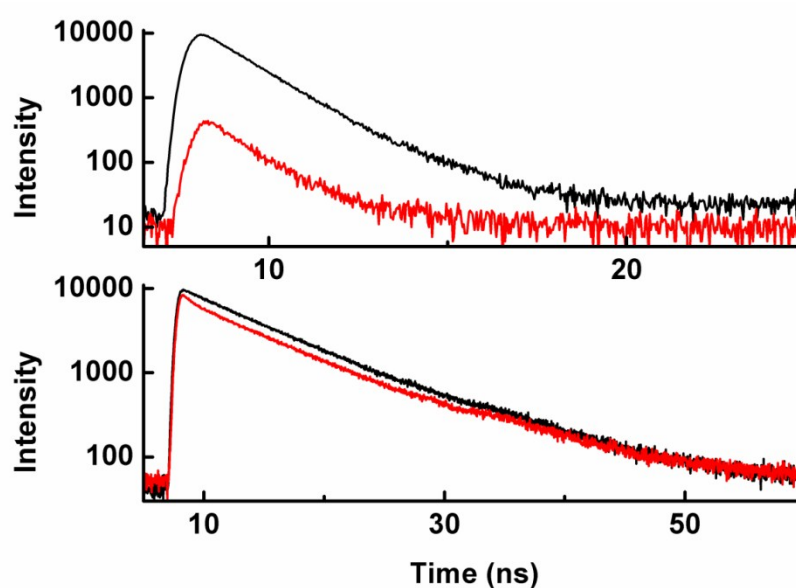


**Figure S20.** Emission decays of ZnTPP, compound **2** (up) and H<sub>2</sub>TPP, compound **3** (down) in CS<sub>2</sub> solution. The fluorescence experiment was carried at 430 nm excitation wavelength.

**Table S3.** Fluorescence Lifetime ( $\tau_{\text{ns}}$ )<sup>a</sup>, Charge-Separation Rate Constant ( $k_{\text{CS}}^s$ )<sup>b</sup> and Charge-Separation Quantum Yield ( $\Phi_{\text{CS}}^s$ )<sup>c</sup> for the C<sub>70</sub>-MTPP system in CS<sub>2</sub> solution.

	$\tau_{\text{ns}}$	$k_{\text{CS}}^s \text{ s}^{-1}$	$\Phi_{\text{CS}}^s$
H <sub>2</sub> TPP	6.68		
<b>3</b>	6.57	$2.415 \times 10^6$	0.016
ZnTPP	1.30		
<b>2</b>	1.13	$1.187 \times 10^8$	0.134

<sup>a</sup> Fluorescence Lifetime was performed in CS<sub>2</sub> solution; <sup>b</sup>  $k_{\text{CS}}^s = (1/\tau_{\text{COMPLEX}}) - (1/\tau_{\text{MTPP}})$ ; <sup>c</sup>  $[(1/\tau_{\text{COMPLEX}}) - (1/\tau_{\text{MTPP}})] / (1/\tau_{\text{COMPLEX}})$

**Table S4.** Binding constant obtained from  $^1\text{H}$  NMR, UV-vis titration and fluorescence titration of a series of similar structure compounds.

	$^1\text{H}$ NMR titration	UV-vis titration	Fluorescence titration	Solvent	Ref.
$\text{C}_{63}\text{H}_{54}\text{CoN}_4\text{P} \cdot \text{C}_{60}$	79			$\text{CHCl}_3/\text{CS}_2$	11
$\text{C}_{63}\text{H}_{54}\text{CoN}_4\text{P} \cdot \text{C}_{70}$	605			$\text{CHCl}_3/\text{CS}_2$	11
$\text{C}_{28}\text{H}_{36}\text{N}_4 \cdot \text{C}_{60}$		43700		Toluene	10
$\text{C}_{28}\text{H}_{36}\text{N}_4 \cdot \text{C}_{70}$		247350		Toluene	10
$\text{C}_{28}\text{H}_{36}\text{N}_4 \cdot \text{C}_{60}$		303725		chloroform	10
$\text{C}_{28}\text{H}_{36}\text{N}_4 \cdot \text{C}_{70}$		1430335		chloroform	10
$\text{C}_{28}\text{H}_{36}\text{N}_4 \cdot \text{C}_{60}$		84980		<i>o</i> -DCB	10
$\text{C}_{28}\text{H}_{36}\text{N}_4 \cdot \text{C}_{70}$		586650		<i>o</i> -DCB	10
$\text{C}_{28}\text{H}_{36}\text{N}_4 \cdot \text{C}_{60}$		153400		benzonitrile	10
$\text{C}_{28}\text{H}_{36}\text{N}_4 \cdot \text{C}_{70}$		479150		benzonitrile	10
$\text{C}_{80}\text{H}_{60}\text{N}_4\text{Zn} \cdot \text{C}_5\text{H}_5\text{N} \cdot \text{C}_{60}$	10000	11000		<i>o</i> -DCB	9
$\text{C}_{80}\text{H}_{60}\text{N}_4\text{Zn} \cdot \text{C}_5\text{H}_5\text{N} \cdot \text{C}_{70}$	12000	13000		<i>o</i> -DCB	9
$\text{H}_2\text{TPP} \cdot 2\text{OMe} \cdot \text{C}_{60}$		1300		Toluene	8
$\text{H}_2\text{TPP} \cdot 3\text{OMe} \cdot \text{C}_{60}$		1400		toluene	8
$\text{H}_2\text{TPP} \cdot \text{C}_{60}$		220		toluene	8
$\text{CoTPP} \cdot \text{C}_{70}$ ( <b>1</b> )	2610 <sup>a</sup>	5900		$\text{CS}_2$	This work
$\text{H}_2\text{TPP} \cdot \text{C}_{70}$ ( <b>3</b> )		7500	13300	$\text{CS}_2$	This work
$\text{ZnTPP} \cdot \text{C}_{70}$ ( <b>2</b> )		4800	18200	$\text{CS}_2$	This work

[a] Measured in  $\text{CS}_2/\text{CDCl}_3$  (1/1).

Also, to further understand the interaction between  $\text{C}_{70}$  and  $\text{M}(\text{TPP})$ , the classic titration methods including UV-Vis,  $^1\text{H}$ -NMR and steady-state fluorescence spectra were performed. For comparison purpose, a series of binding constants of similar structures were listed in Table S3. binding constant of this type of supramolecular aggregates shows big difference using different solvents, as different stacking mode could formed. As shown in Fig S14-S16, the different absorption band in S and Q band of  $\text{H}_2(\text{TPP})$ ,  $\text{Co}(\text{TPP})$  and  $\text{Zn}(\text{TPP})$  are caused by coordination between Co or Zn and N belonged to pyrrole rings in UV-vis spectra. When  $\text{C}_{70}$  was added into the  $\text{H}_2\text{TPP}$  solution, one peak at 419 nm in S band and four peaks at 514 nm, 548 nm, 592 nm and 649 nm respectively in Q band can be assigned to  $\text{H}_2\text{TPP}$ , and the intensity of these peaks were all observed to be increased. Besides, the peaks at S and Q band were also found to be blue-shifted after titrating  $\text{C}_{70}$ , due to the interaction forces between  $\text{C}_{70}$  molecules and  $\text{H}_2\text{TPP}$  molecules. Based on this, Benesi-Hildebrand equation<sup>1</sup> was used to calculate the binding constant, which was  $7.5 \times 10^3 \text{ M}^{-1}$ . The same phenomenon was also found after titrating  $\text{C}_{70}$  into  $\text{Zn}(\text{TPP})$  solution and  $\text{Co}(\text{TPP})$  solution and the binding constant was  $4.8 \times 10^3 \text{ M}^{-1}$  and  $5.9 \times 10^3 \text{ M}^{-1}$ , respectively. These binding constant values were closed to the similar systems<sup>2</sup> and

smaller than the fullerene-porphyrin system whose binding force was coordinate bond.<sup>3,4</sup> Also, the steady-state fluorescence spectra titration was utilized by adding C<sub>70</sub> into the MTPP solution (shown in Fig. S17 and S18). The fluorescence of H<sub>2</sub>TPP in the CS<sub>2</sub> solution shows the characteristic emission at 657 nm and 717 nm upon 430 nm excitation. When C<sub>70</sub> was added into the H<sub>2</sub>TPP, no shifts but only quenching was observed. According to Benesi-Hildebrand equation, binding constant of compound **3** was calculated to be  $1.33 \times 10^4 \text{ M}^{-1}$ . Unlike H<sub>2</sub>(TPP), Zn(TPP) exhibits the characteristic emission at 600 nm and 646 nm upon 430 nm. The different emission is caused by the addition of Zn<sup>2+</sup>, which changes the emission spectrum of porphyrin. The binding constant of compound **2** was calculated by using Benesi-Hildebrand equation to be  $1.82 \times 10^4 \text{ M}^{-1}$ . Compared with the binding constant obtained by UV-vis titration, the binding constant obtained by fluorescence titration is a little bigger. This difference was also found in previous studies<sup>5,6</sup>, and can be considered to be acceptably close. Solid-stated fluorescence spectra (Fig. S19) was used to investigate the difference between different states. Compared with solvent state, the emission of Zn(TPP) and compound **2** are both red-shifted to 653 nm and 719 nm, respectively. As for H<sub>2</sub>(TPP) and compound **3**, the peaks at 657 nm and 717 nm are still can be observed. Besides, H<sub>2</sub>TPP and compound **3** both show the emission peak at 755 nm, which is not found in the solvent state. Considering the same arrangement of compound **2** and **3**, the appeared peak may be caused by changing the dipole moment of porphyrin molecular after the addition of Zn<sup>2+</sup>. The emission decay profiles of the MTPP (M = H<sub>2</sub> and Zn) and C<sub>70</sub> were shown in Fig. S20. Similar to the changes of fluorescence spectra, when Zn<sup>2+</sup> was coordinated to porphyrin molecular, the lifetime ( $\tau_{ns}$ ) of Zn(TPP) (1.30 ns) and compound **3** (1.13 ns) is much shorter than that of H<sub>2</sub>(TPP) (6.67 ns) and **2** (6.57 ns). Given that the fluorescence quenching is caused by charge separation from the singlet excited MTPP to C<sub>70</sub>, Charge-Separation Rate Constant ( $k_{cs}^s$ ) and Charge-Separation Quantum Yield ( $\Phi_{CS}^s$ ) were evaluated (as shown in Table S3) from fluorescent lifetime. The  $k_{cs}^s$  and  $\Phi_{CS}^s$  of compound **2** are much lower than that of compound **3**, indicating that the occurrence of electron transfer is related to the metal in the co-crystal system. Compared with other fullerene-porphyrin systems, the  $k_{cs}^s$  and  $\Phi_{CS}^s$  of **3** and **2** are lower because of the low bonding force according to binding constant in CS<sub>2</sub> solution.

## 7. Powder X-ray diffraction analysis.

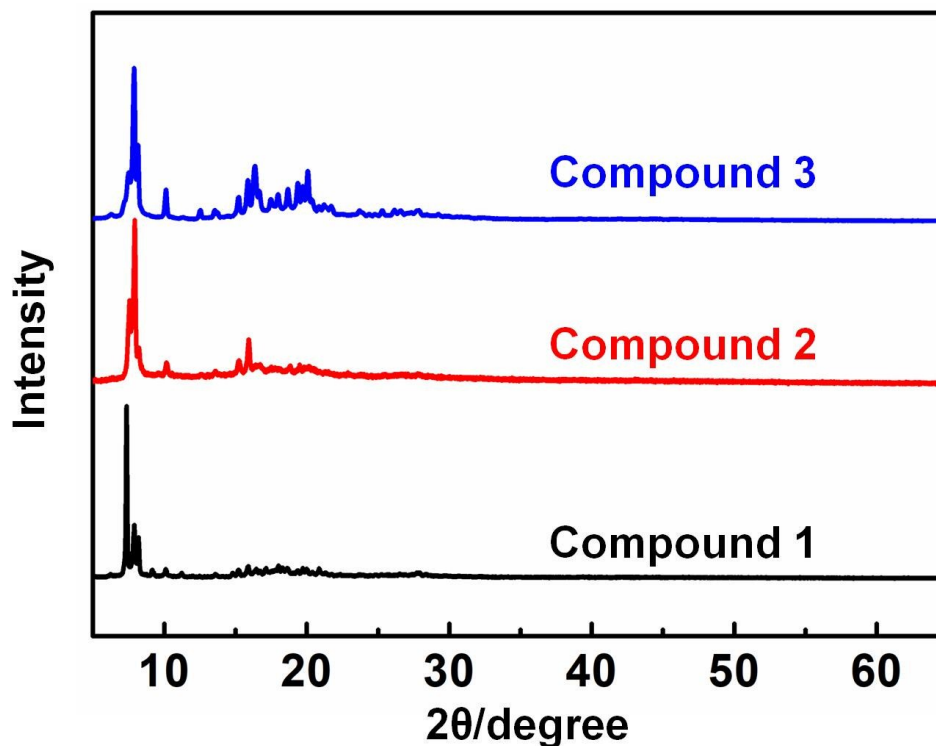


**Figure S21.** PXRD patterns for compound 1 (black), compound 2 (red), compound 3 (blue).

Powder X-ray diffraction (PXRD) measurements were carried out to determine the molecular packing in these three compounds. In the profile of compound 3, a strong peak at  $7.89^\circ$  together with some relatively weaker peaks at  $8.16^\circ$ ,  $16.36^\circ$  and  $20.36^\circ$  were observed, which were assigned to (1-11), (-101), (300) and (024) diffractions. As for compound 2, peaks at  $7.57^\circ$ ,  $7.95^\circ$ ,  $15.94^\circ$  were observed, which were assigned to (1-11), (-101) and (023). Compare to previous work,<sup>7</sup> the direction of crystal growth is much different because of different solvent system. Thus, different solvent can change not only the microscopic structure of molecules but also can the macrostructure. In addition, in the profile of compound 1, peaks at  $7.73^\circ$ ,  $7.91^\circ$ ,  $8.19^\circ$  were observed, which were assigned to (020), (002) and (201).

## 8. Electrochemistry data

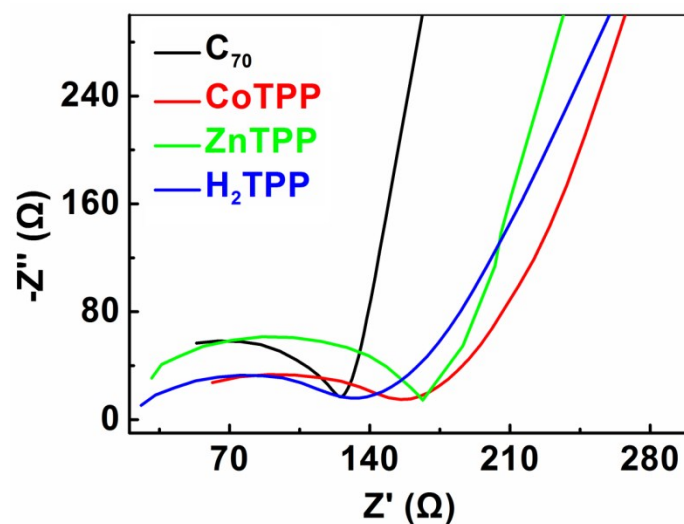


Figure S22. Impedance plots of  $C_{70}$ , CoTPP, ZnTPP and  $H_2$ TPP.

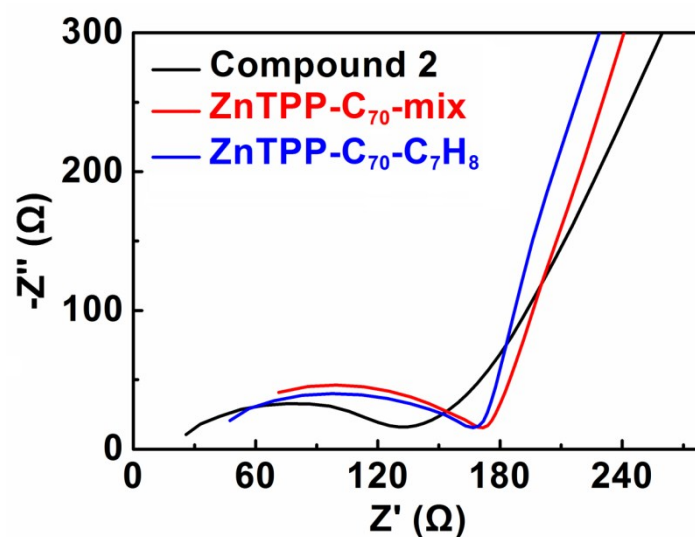


Figure S23. Impedance plots of Compound 2, ZnTPP- $C_{70}$ - $C_7H_8$  and ZnTPP- $C_{70}$ -mix.

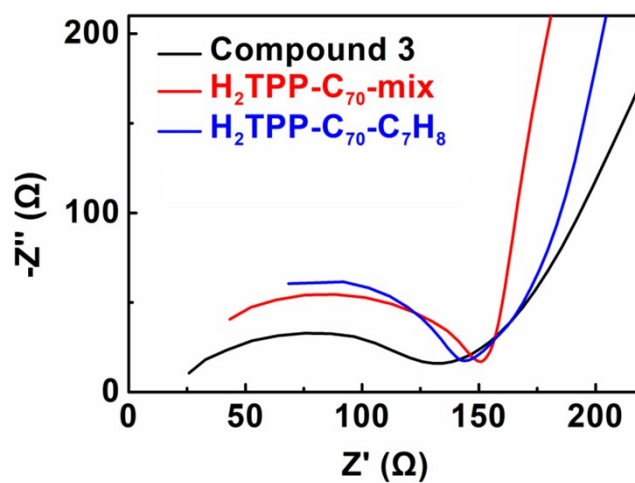
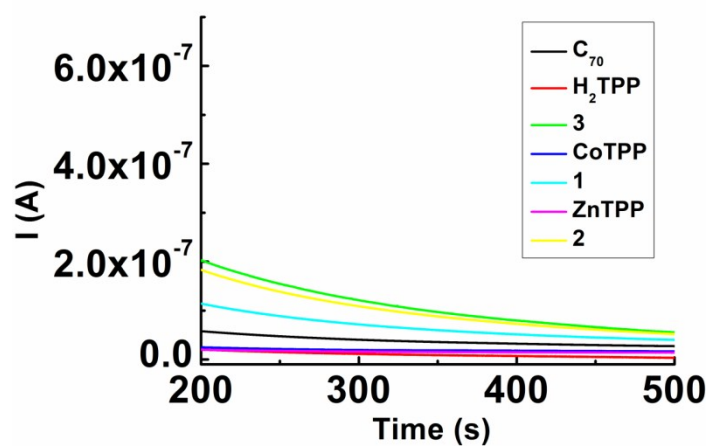


Figure S24. Impedance plots of Compound 3,  $H_2$ TPP- $C_{70}$ - $C_7H_8$  and  $H_2$ TPP- $C_{70}$ -mix.

**Table S5.**  $R_s$  and  $R_{ct}$  of different compounds.

Compound	$R_s / \Omega$	$R_{ct} / \Omega$
$C_{70}$	125.4	115.4
$H_2TPP$	185.6	157.0
ZnTPP	113.6	100.2
CoTPP	157.6	129.0
<b>1</b>	140.3	127.6
<b>2</b>	165.7	149.4
<b>3</b>	132.3	105.4
CoTPP- $C_{70}$ - $C_7H_8$	180.1	128.0
ZnTPP- $C_{70}$ - $C_7H_8$	172.3	158.6
$H_2TPP$ - $C_{70}$ - $C_7H_8$	144.8	128.6
CoTPP- $C_{70}$ -mix	168.3	141.2
ZnTPP- $C_{70}$ -mix	172.9	153.8
$H_2TPP$ - $C_{70}$ -mix	153.7	141.1



**Figure S25.** i-t curve of  $C_{70}$  (black),  $H_2TPP$  (red), **3** (green), CoTPP (blue), **1** (cyan), ZnTPP (magenta) and **2** (yellow) at constant voltage 0.5V during 200 to 500s.

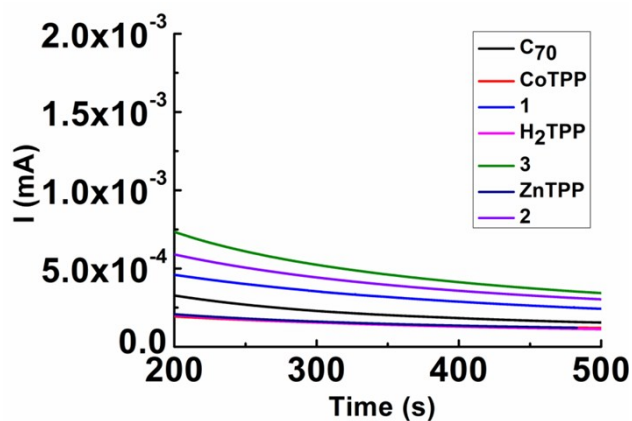


**Figure S26.** i-t curve of C<sub>70</sub> (black), H<sub>2</sub>TPP (red), **3** (green), CoTPP (blue), **1** (cyan), ZnTPP (magenta) and **2** (yellow) at constant voltage 1V during 200 to 500s.

**Table S6.** The current value of different compounds at 250 s, 0.5 V.

Compound	Current (A) *10 <sup>7</sup>
C <sub>70</sub>	0.47465
H <sub>2</sub> TPP	0.2153
ZnTPP	0.1776
CoTPP	0.1517
<b>1</b>	1.545
<b>2</b>	1.386
<b>3</b>	0.8856
CoTPP-C <sub>70</sub> -C <sub>7</sub> H <sub>8</sub>	0.1381
ZnTPP-C <sub>70</sub> -C <sub>7</sub> H <sub>8</sub>	0.09273
H <sub>2</sub> TPP-C <sub>70</sub> -C <sub>7</sub> H <sub>8</sub>	0.05449
CoTPP-C <sub>70</sub> -mix	0.04485
ZnTPP-C <sub>70</sub> -mix	0.1979
H <sub>2</sub> TPP-C <sub>70</sub> -mix	0.639

## 9. The examples of different packing models

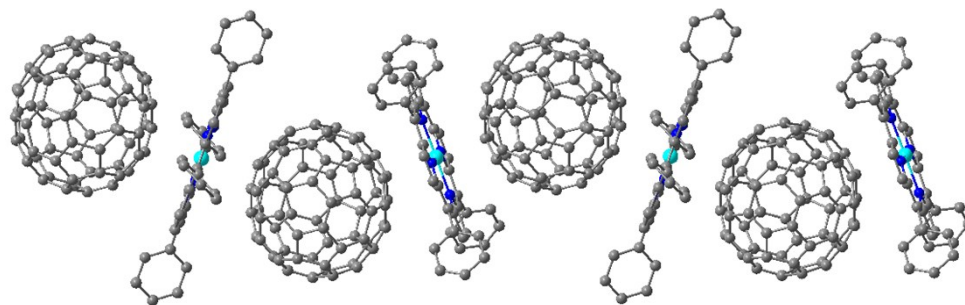


**Figure S27.** View of the packing of ZnTPP-C<sub>70</sub> structure according reference **18** (Wang, B.-Z.; Zheng, S.-S.; Saha, A.; Bao, L.-P.; Lu, X.; Guldi, D. M. Understanding Charge-Transfer Characteristics in Crystalline Nanosheets of Fullerene/(Metallo)porphyrin Cocrystals. *J. Am. Chem. Soc.*, 2017, 139, 10578–10584.). C, gray; Zn, cyan; N, blue.

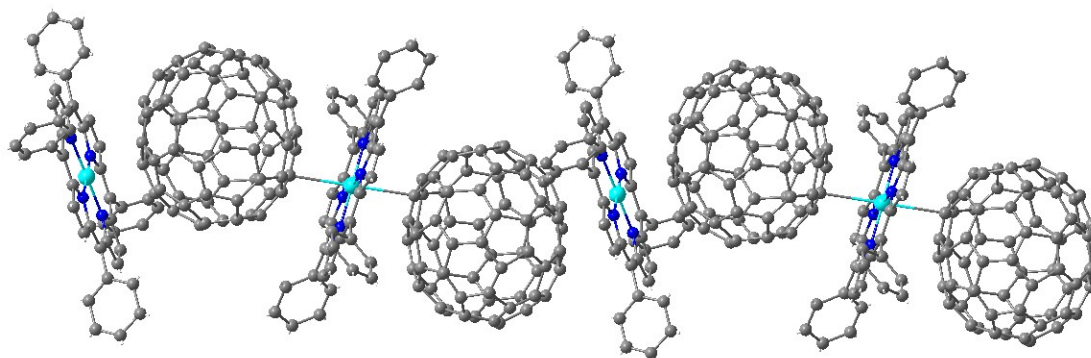


**Figure S28.** View of the packing of ZnTPP-C<sub>70</sub> structure according previous reference (P.D.W.Boyd, M.C.Hodgson, C.E.F.Rickard, A.G.Oliver, L.Chaker, P.J.Brothers, R.D.Bolskar, F.S.Tham, C.A.Reed (1999) *J.Am.Chem.Soc.*, 121, 10487.). C, gray; Zn, cyan; N, blue.

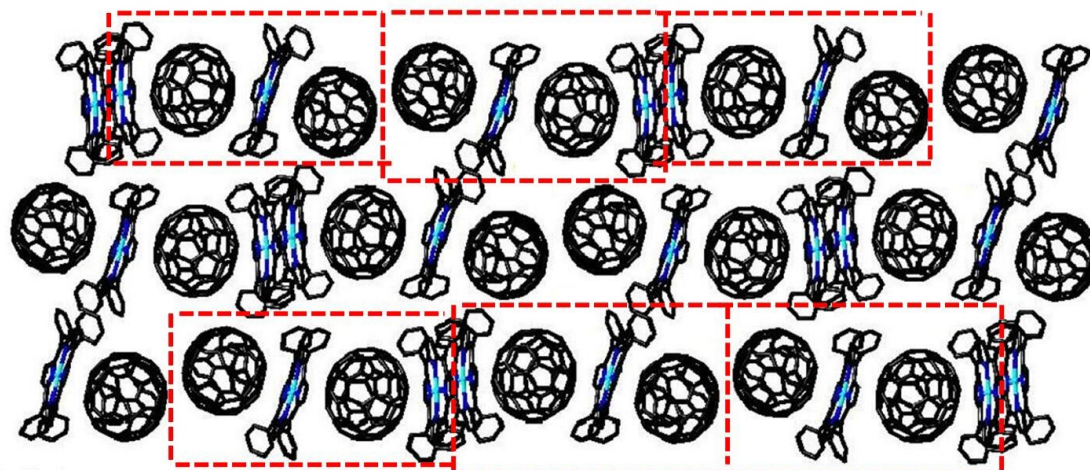


**Figure S29.** View of the packing of **2**. Hydrogen atoms and CS<sub>2</sub> molecules are removed for clarity. C, gray; Co, red; N, blue; Zn, cyan.

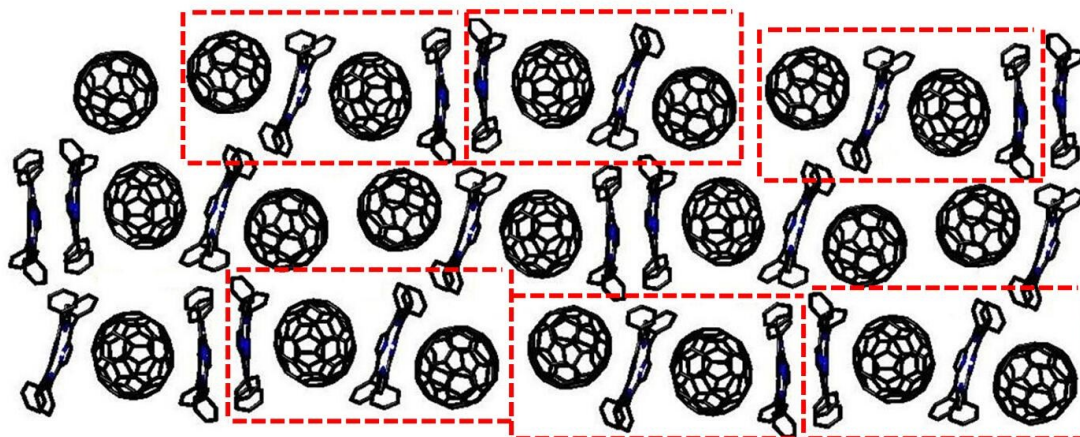


**Figure S30.** View of the packing of **3**. Hydrogen atoms and CS<sub>2</sub> molecules are removed for clarity. C, gray; Co, red; N, blue.

As can be seen from Figure S27 and S28, the packing way of fullerene and porphyrin molecular of previous work is like ABAB-type and it is mentioned as zigzag chain type as shown in Scheme 1 (d). But in our work, a new packing way was found as shown in Figure R3 and R4 and it can be describe as ABABBABA-type. That's why we call it Dimer Type (Scheme 1 (e)). Because of this structural difference, the resistances of different compounds were shown differences.

## References

- (1) (a) Benesi, H. A.; Hildebrand, J. H. A Spectrophotometric Investigation of the Interaction of Iodine with Aromatic Hydrocarbons. *J. Am. Chem. Soc.*, **1949**, 71, 2703-2707. (b) Barra, M.; Bohne, C.; Scaiano, J. C. Effect of Cyclodextrin Complexation on The Photochemistry of Xanthone. Absolute Measurement of The Kinetics for Triplet-State Exit. *J. Am. Chem. Soc.*, **1990**, 112, 8075-8579.
- (2) Ayabe, M.; Ikeda, A.; Shinkai, S.; Sakamoto, S.; Yamaguchi, K. A Novel [60]fullerene Receptor with A Pd(II)-Switched Bisporphyrin Cleft. *Chem. Commun.*, **2002**, 10, 1032–1033.
- (3) Wilson, S. R.; MacMahon, S.; Tat, F. T.; Jarowski, P. D.; Schuster, D. I. Synthesis and Photophysics of A linear Non-Covalently Linked Porphyrin-Fullerene Dyad. *Chem. Commun.*, **2003**, 34, 226–227.
- (4) Ei-Khouly, M. E.; Wijesinghe, C. A.; Nesterov, V. N.; Zandler, M. E.; Fukuzumi, S.; D'Souza, F. Ultrafast Photoinduced Energy and Electron Transfer in Multi-Modular Donor–Acceptor Conjugates. *Chem. Eur. J.*, **2012**, 18, 13844-13853.
- (5) Sakaguchi, K.; Kamimura, T.; Uno, H.; Mori, S.; Ozako, S.; Nobukuni, H.; Ishida, M.; Tani, F. Phenothiazine-Bridged Cyclic Porphyrin Dimers as High-Affinity Hosts for Fullerenes and Linear Array of C<sub>60</sub> in Self-Assembled Porphyrin Nanotube. *J. Org. Chem.*, **2014**, 79, 2980–2992.
- (6) D'Souza, F.; Chitta, R.; Gadde, S.; Zandler, M. E.; McCarty, A. L.; Sandanayaka, A. S. D.; Araki, Y.; Ito, O. Potassium Ion Controlled Switching of Intra- to

Intermolecular Electron Transfer in Crown Ether Appended Free-Base Porphyrin-Fullerene Donor-Acceptor Systems. *J. Phys. Chem. A*, **2006**, 110, 4338-4347.

(7) Wang, B. Z.; Zheng, S. S.; Saha, A.; Bao, L. P.; Lu, X.; Guldi, D. M. Understanding Charge-Transfer Characteristics in Crystalline Nanosheets of Fullerene/(Metallo)porphyrin Cocrystals. *J. Am. Chem. Soc.*, **2017**, 139, 10578–10584.

(8) Hiroshi, I.; Masahiro, U.; Soonchul, K.; Hironobu, H.; Shinya, H.; Hironori, K. ; Shu, S.; Akinori, S.; Seiichi, T.; Tomokazu, U.; Yoshihiro, M.; Kaname, Y.; Seiji, I.; Motoo, S.; Nikolai, V. T.; Helge, L. Effects of porphyrin substituents on film structure and photoelectrochemical properties of porphyrin/fullerene composite clusters electrophoretically deposited on nanostructured SnO<sub>2</sub> electrode. *Chem. Eur. J.*, **2010**, 13, 10182-10193.

(9) Saegusa, Y.; Ishizuka, T.; Kojima, T. Frontispiece: Supramolecular Interaction of Fullerenes with a Curved  $\pi$ -Surface of a Monomeric Quadruply Ring-Fused Porphyrin. *Chem. Eur. J.*, **2015**, 21, 5302-5306.

(10) Pal, D.; Goswami, D.; Nayak, S. K.; Chattopadhyay, S.; Bhattacharya, S. Spectroscopic and Theoretical Insights into the Origin of Fullerene–Calix[4]pyrrole Interaction. *J. Phys. Chem. A*, **2010**, 114, 6776-6786.

(11) Chen, C.; Zhu, Y. Z.; Fan, Q. J.; Song, H. B.; Zheng, J. Y. Syntheses of corrole derivatives and their supramolecular interactions with fullerenes in solution and the solid state. *Tetrahedron Letters*, **2013**, 54, 4143-4147.